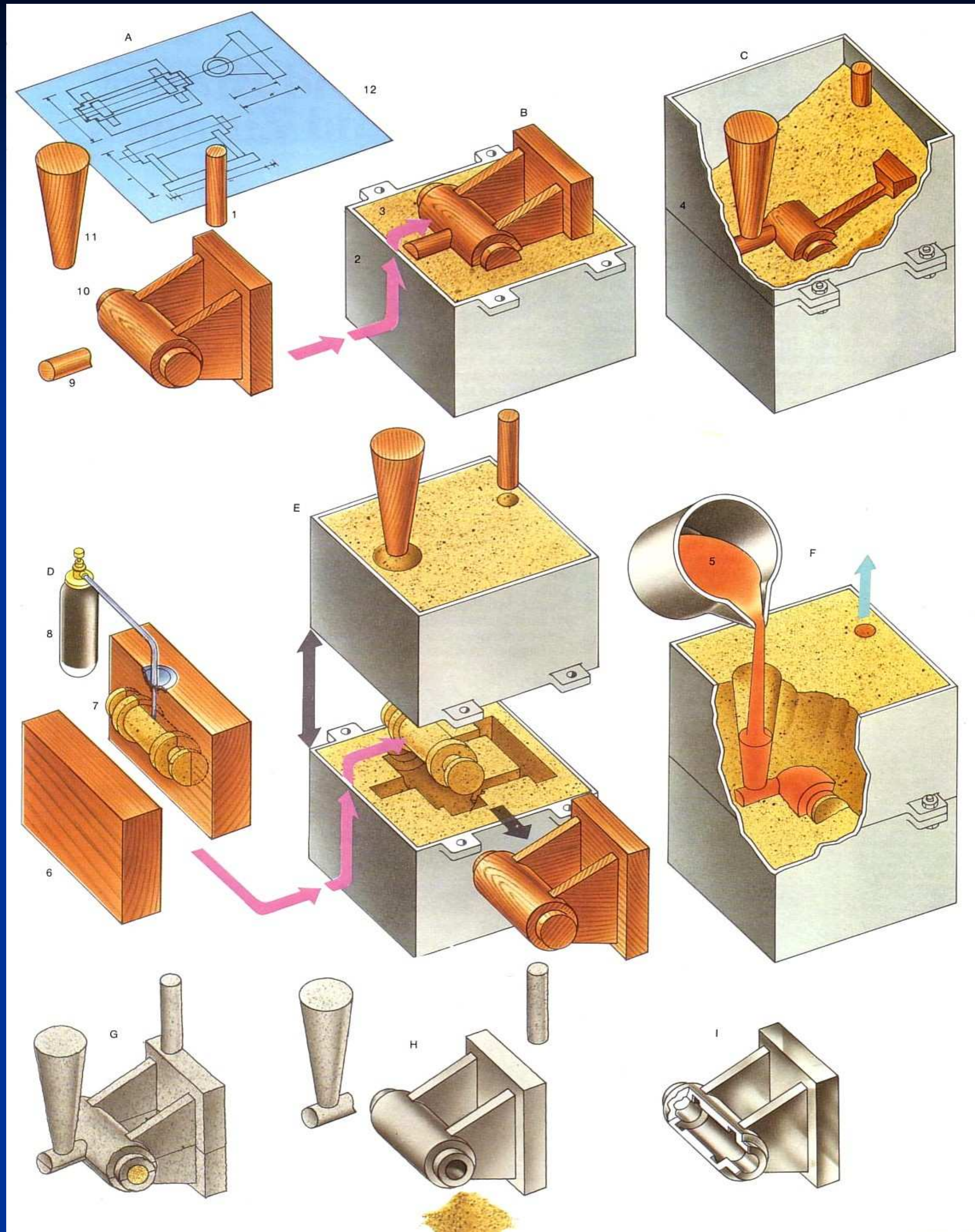
A
12
B
C
1
11
3
2
4
10
9
E
D
8
7
6
5
F
G
H
I

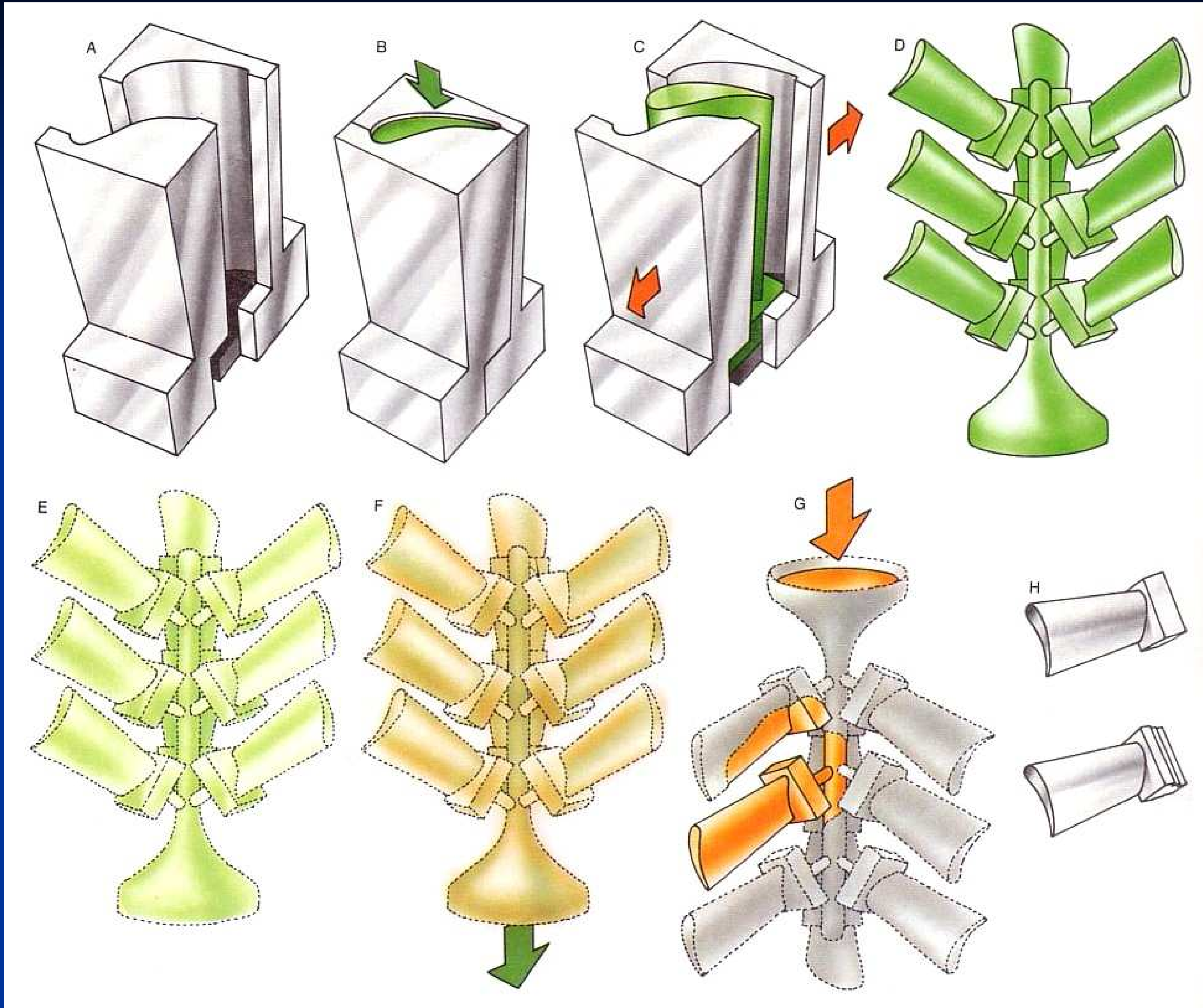
A
B
C
D
E
F
G
H

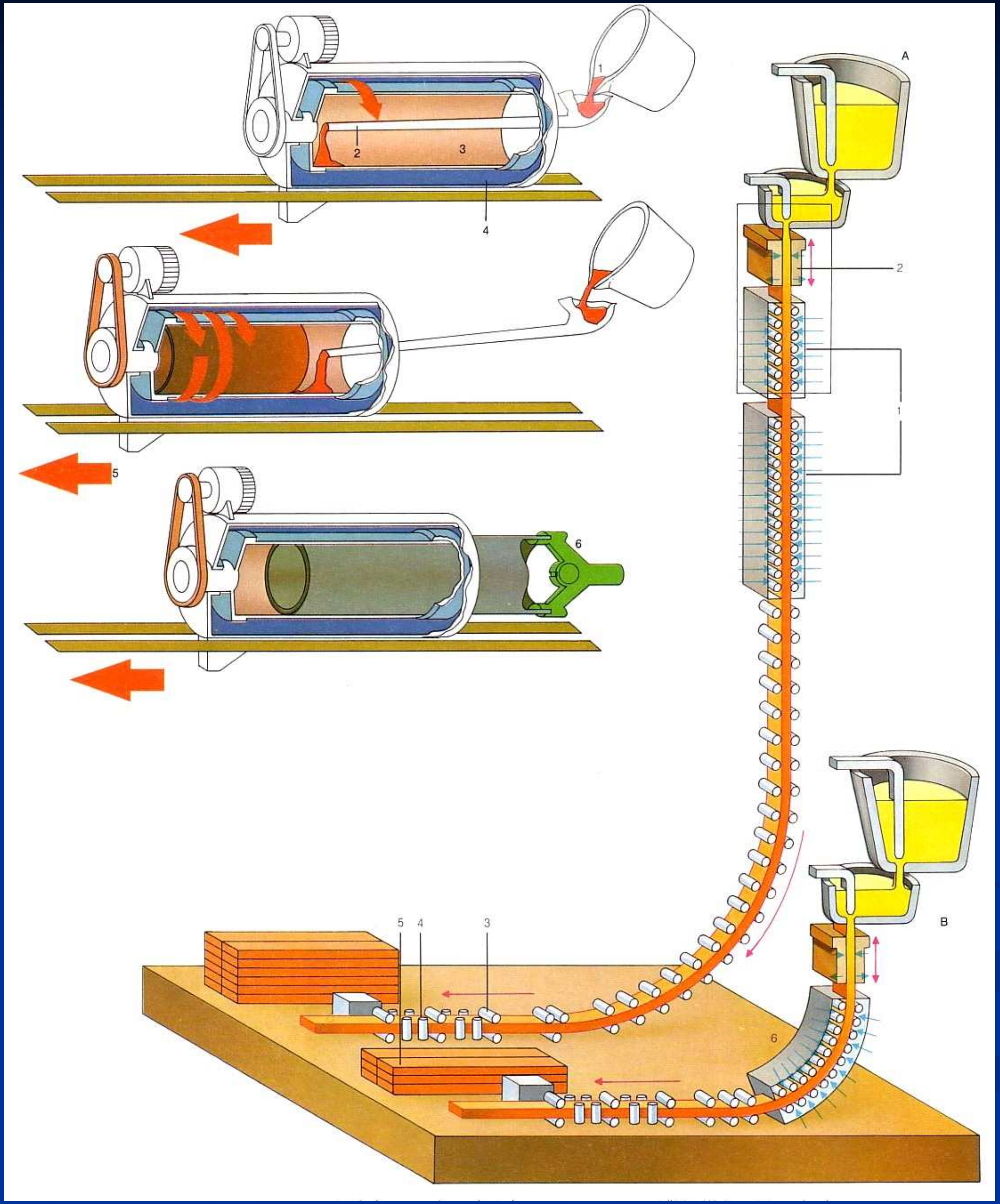
1
2
3
4
5
6
A
B

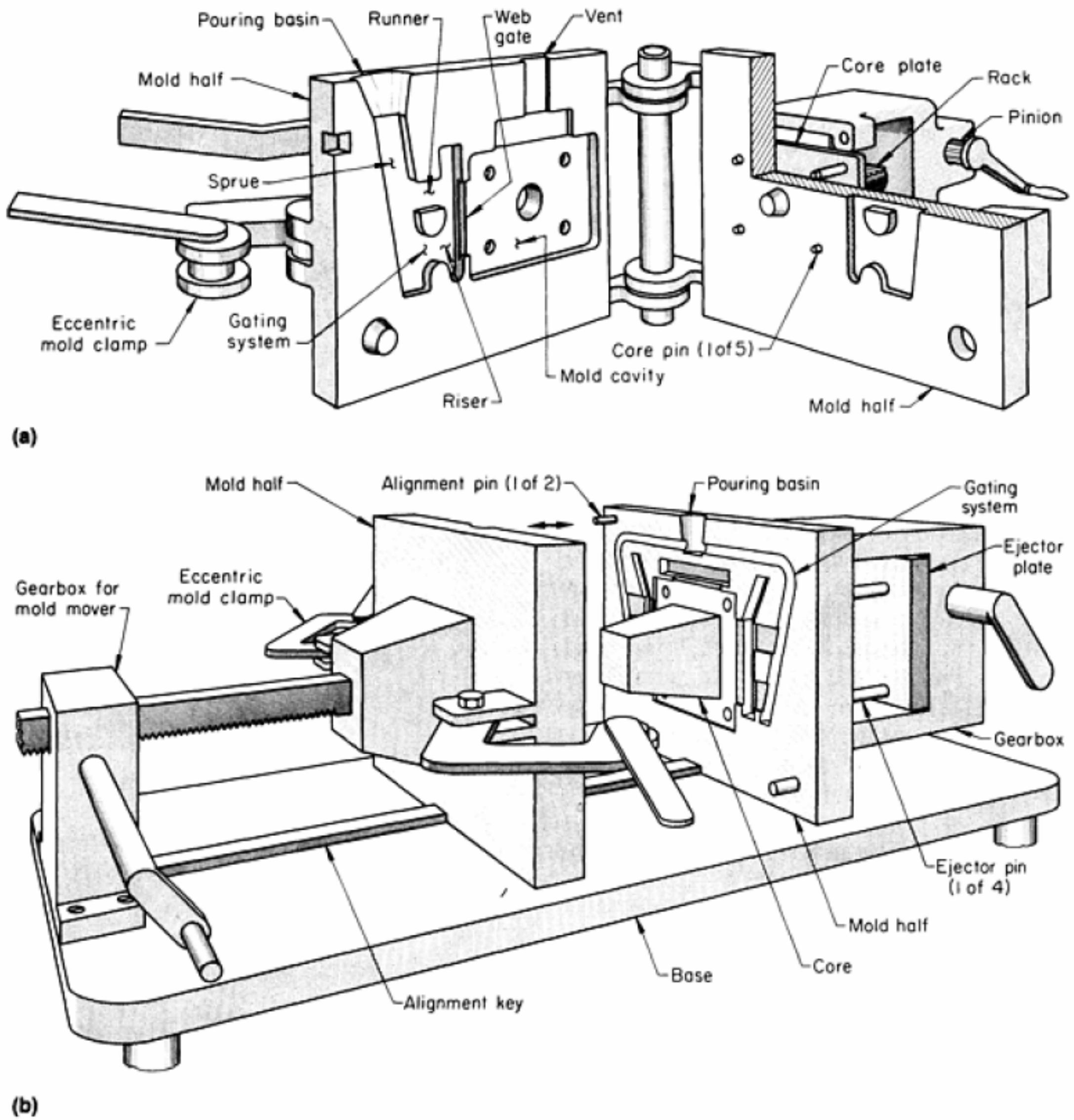

Fig. 2 Two types of manually operated permanent mold casting machines. (a) Simple book-type mold for shallow-cavity castings. (b) Device with straight-line retraction for deep-cavity molds

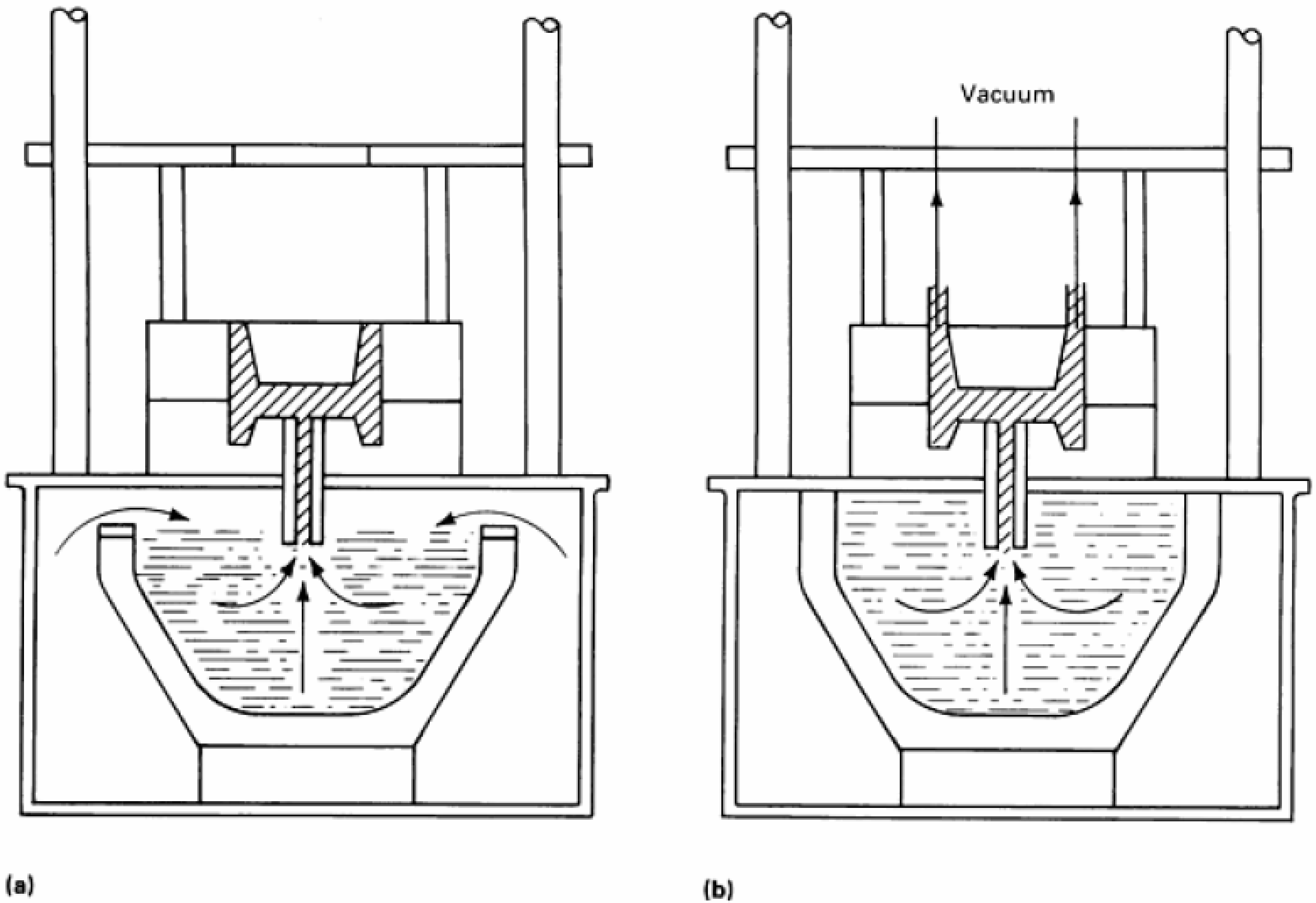

Fig. 5 Schematics of low-pressure (a) and vacuum casting (b) units used with permanent molds

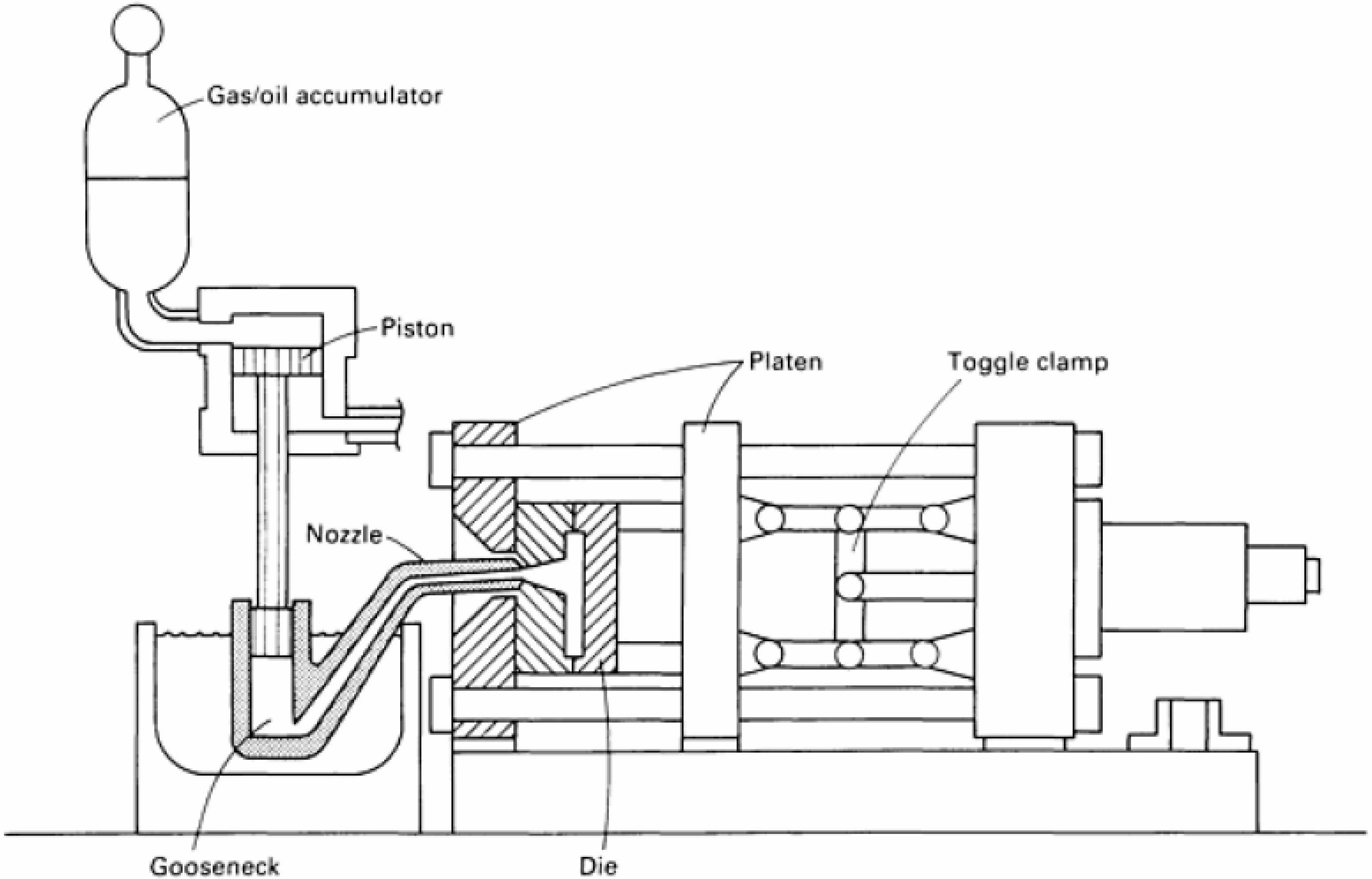

Fig. 1 Schematic showing the principal components of a hot chamber die casting machine

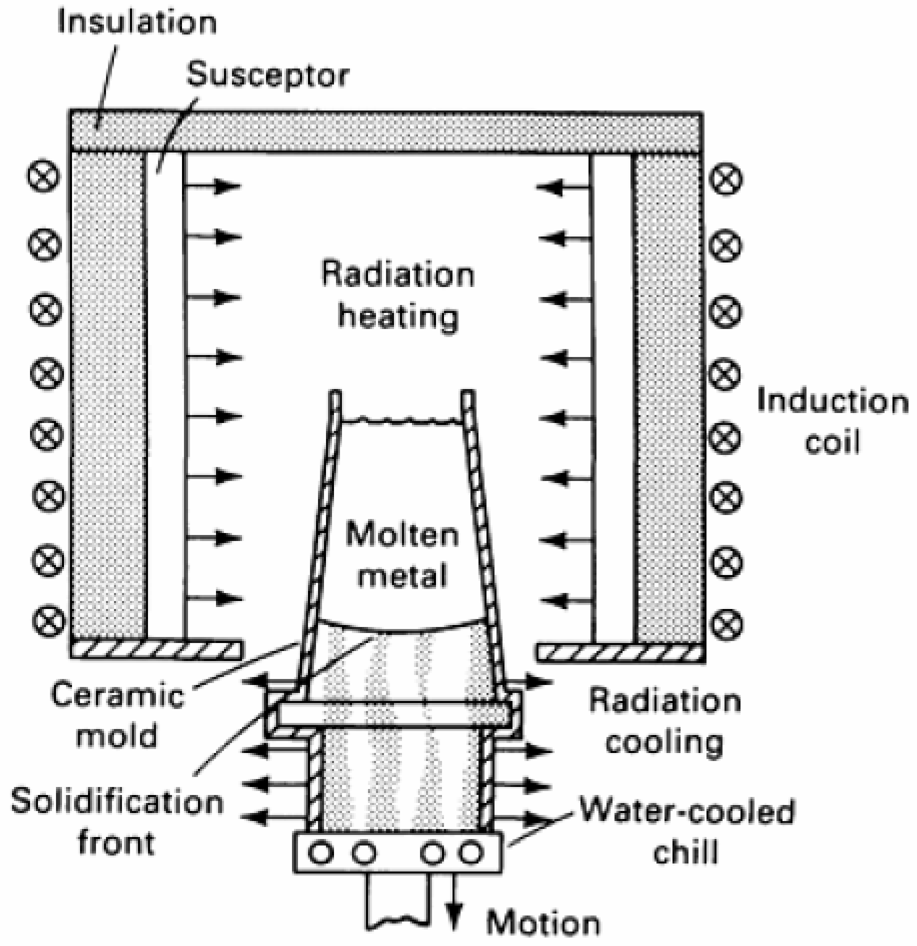

Fig. 3 Schematic showing the directional solidification process. Source: Ref 2

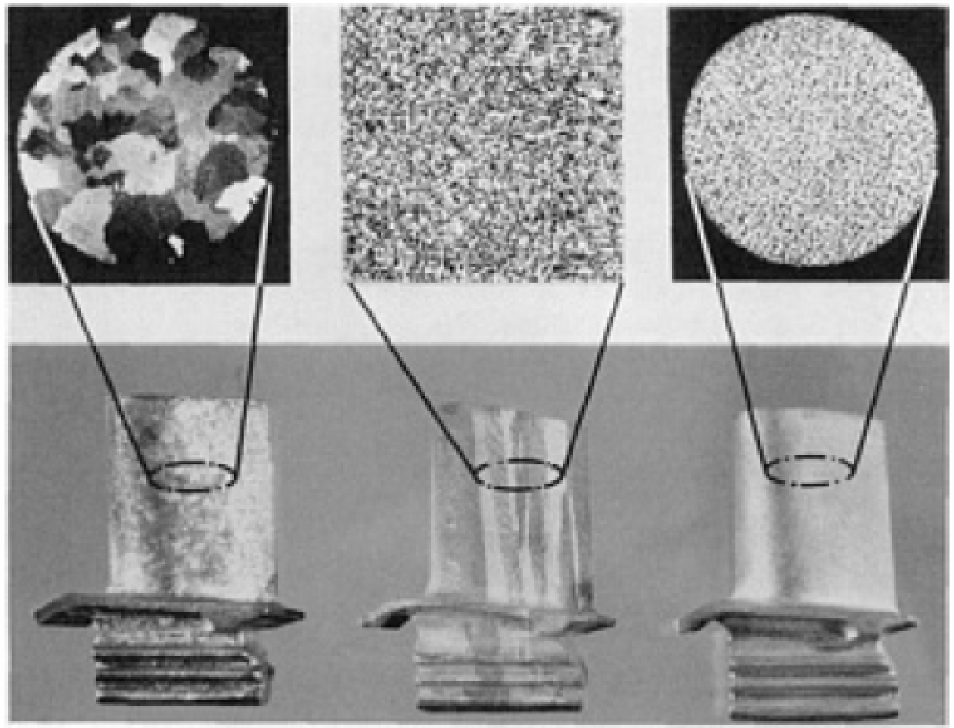

Fig. 5 Comparison of microstructures in (from left) equiaxed, directionally solidified, and single-crystal blades. Courtesy of P.R. Sahm, Giesserei-Institut der RWTH (West Germany)

SOLIDIFICACION DE METALES

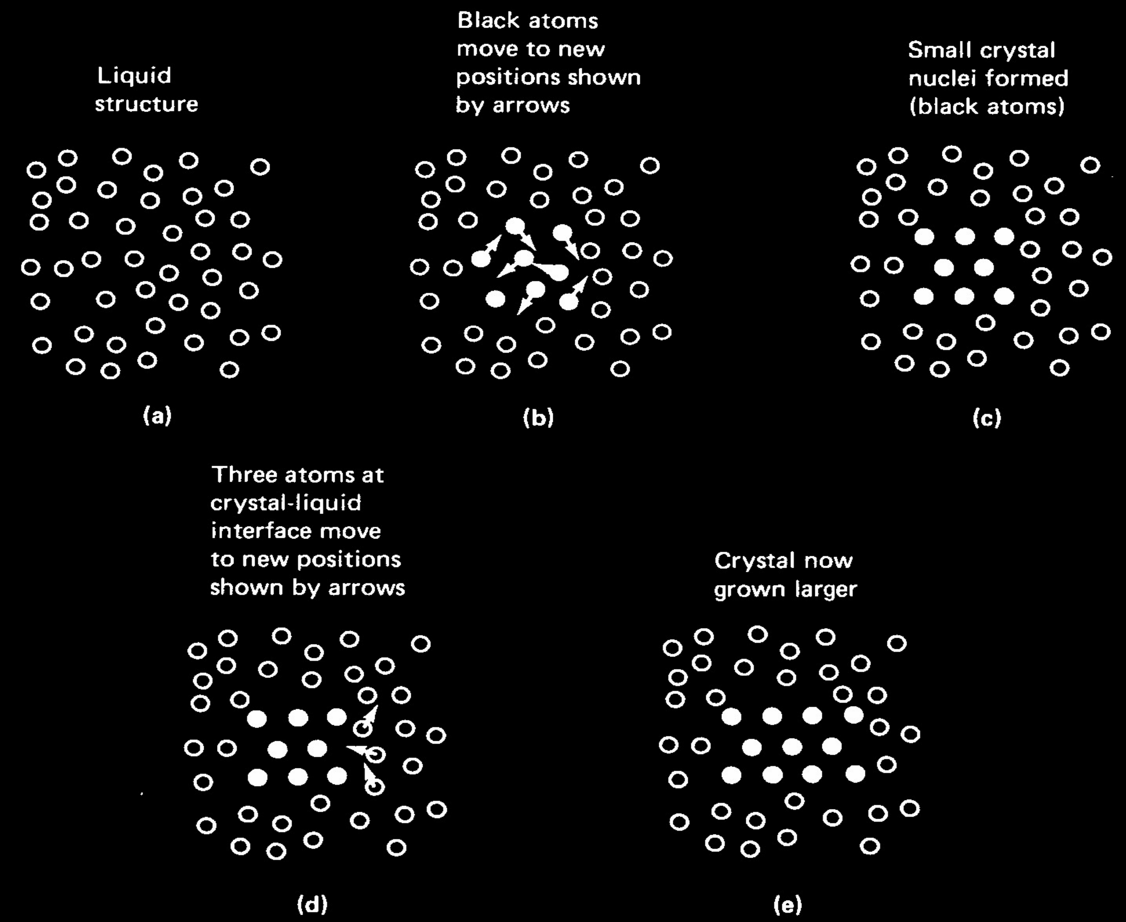

Fig. 2-1. Schematic representation of formation of a crystal nucleus and its growth in a liquid.

FORMACION DE NUCLEOS CRISTALINOS EN EL LIQUIDO

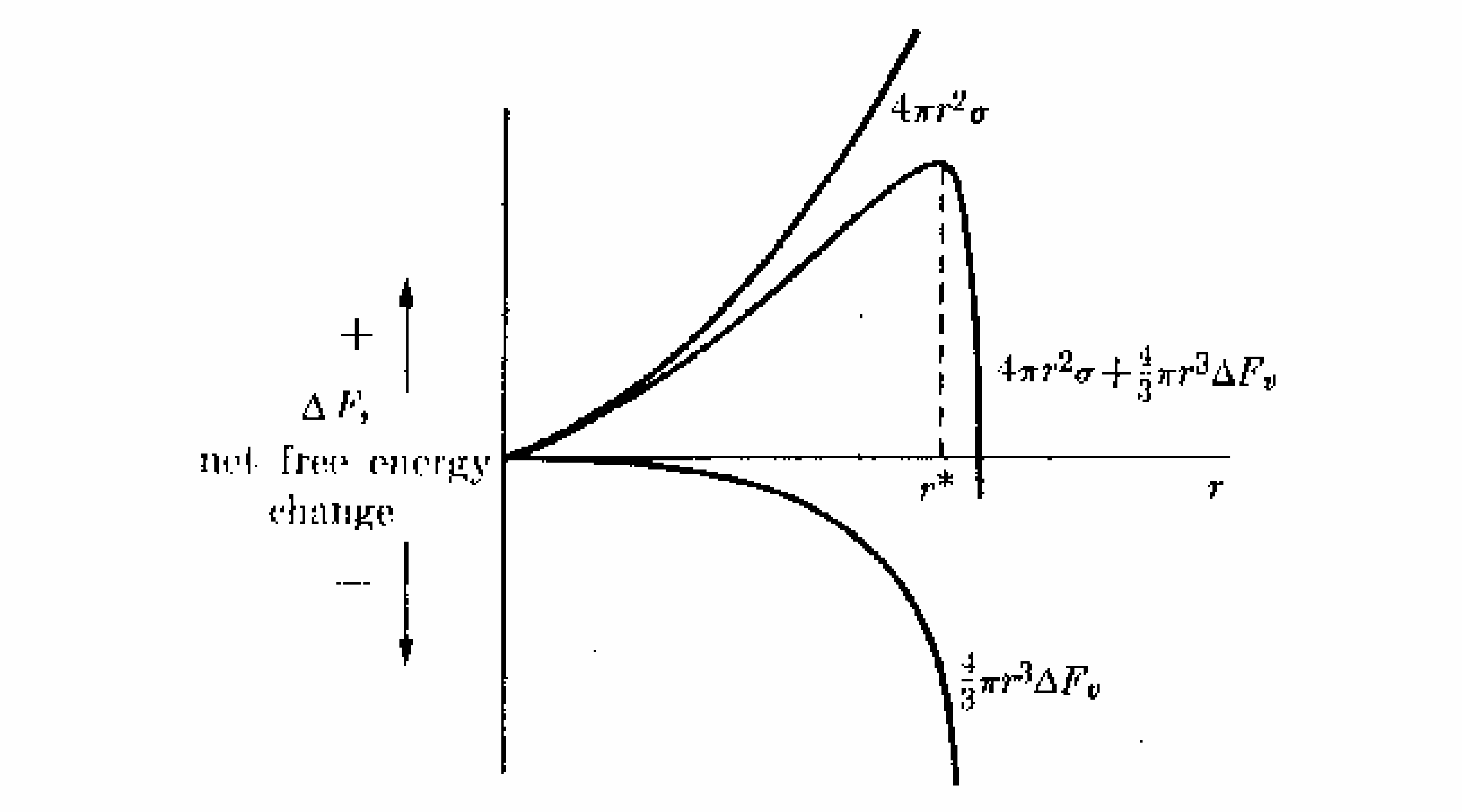

$4\pi r^2\sigma$
$4\pi r^2\sigma + \frac{4}{3}\pi r^3 \Delta F_v$
+
ΔF,
net free energy
change
−
r^*
r
$\frac{4}{3}\pi r^3 \Delta F_v$

SOLIDIFICACION DE METALES

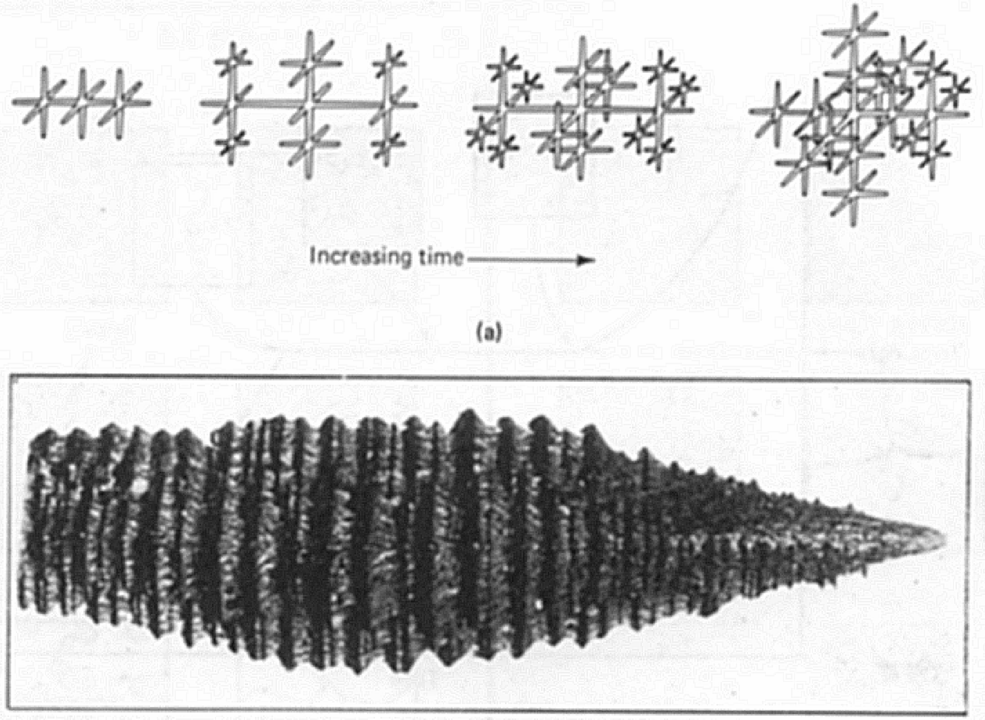

Fig. 2-2. (a) Schematic illustration of the growth of a dendritic crystal (adapted from P. S. Hurd, Metallic Materials, Holt, Rinehart and Winston, New York, 1968). (b) Photograph of a large, 9 in. long, dendrite which formed in a steel (from A. Sauveur, The Metallography and Heat Treatment of Iron and Steel, 4th Ed., The University Press, Cambridge, Eng., 1935).

CRECIMIENTO DENDRÍTICO EN METALES

SOLIDIFICACION DE METALES

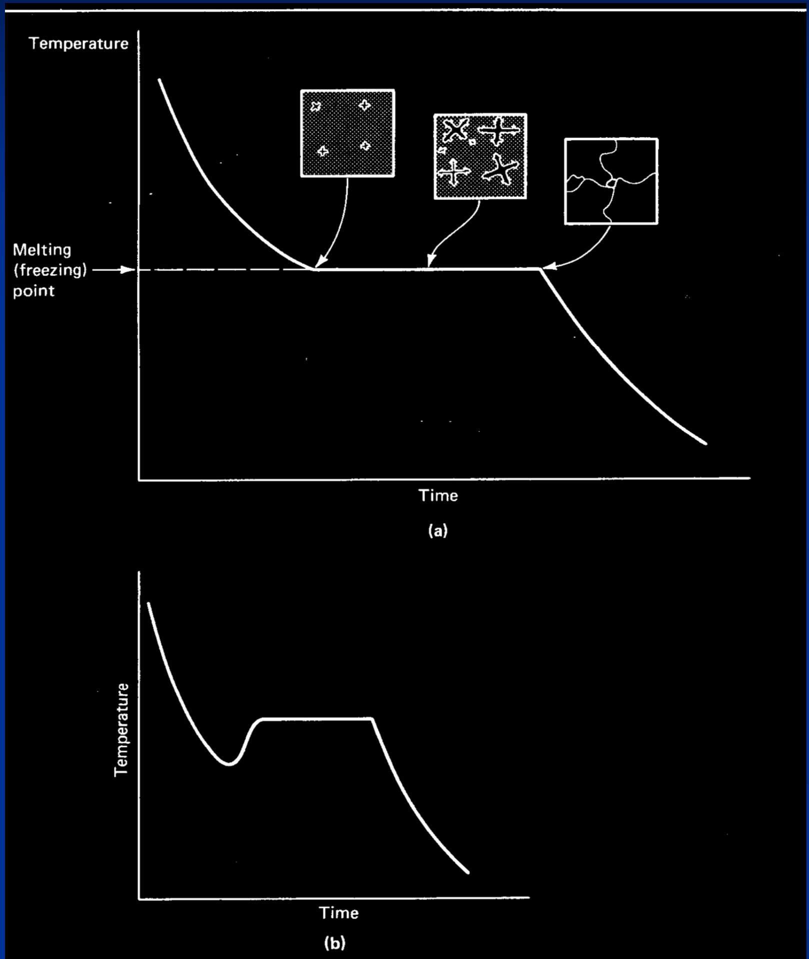

Fig. 2-3. Schematic cooling curves. (a) Curve in which negligible undercooling occurs. (b) Curve showing undercooling.

CURVAS DE ENFRIAMIENTO METAL PURO

SOLIDIFICACION DE METALES

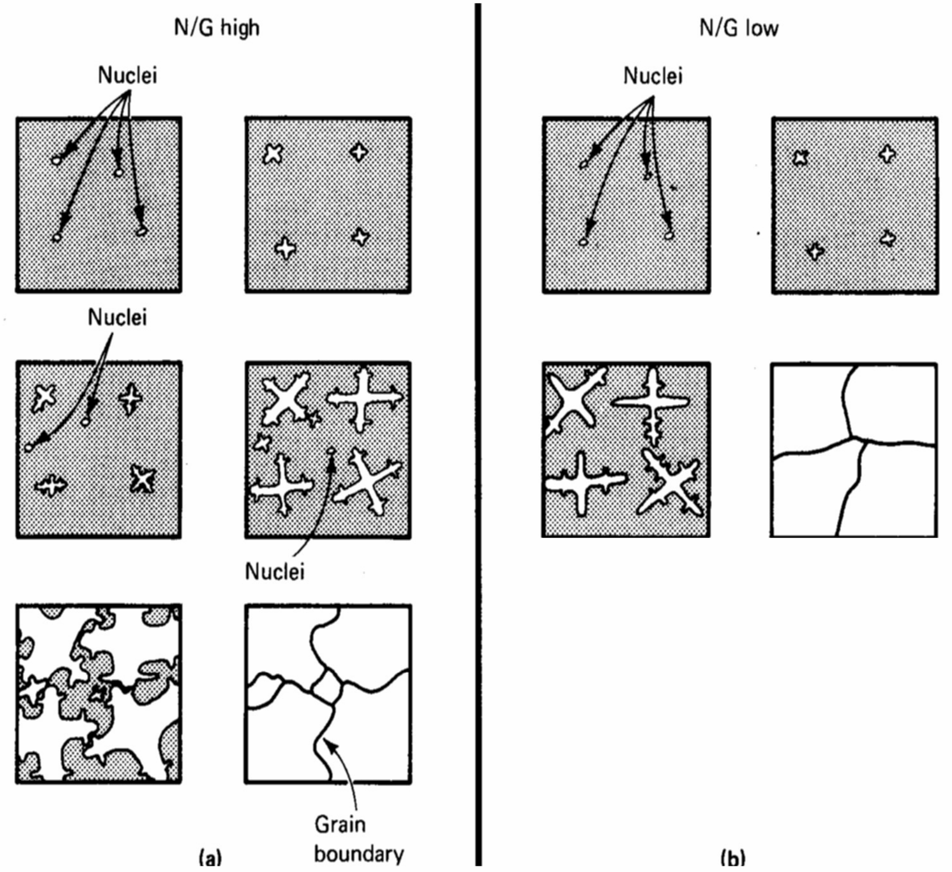

Fig. 2-4. Schematic illustration of the effect of the ratio of the nucleation rate (N) to the growth rate (G) on the final grain size. The lower N/G ratio in (b) gives a larger grain size.

EFECTO DE LA RAZÓN DE NUCLEACION Y VELOCIDAD DE CRECIMIENTO SOBRE EL TAMAÑO DE GRANO

SOLIDIFICACION DE METALES

Fig. 2-5. Effect of addition of a grain refiner on the cast grain size and shape of commercially pure aluminum (1100 aluminum) cast by a two-belt method. Both pictures are of longitudinal sections, shown at actual size. The upper slab was cast without a grain refiner and the lower with a grain refiner addition (e.g., titanium or titanium and boron). (From Metals Handbook, 8th Ed., Vol 8, American Society for Metals, Metals Park, Ohio, 1973)

EFECTO DE AFINANTES SOBRE EL TAMAÑO DE GRANO EN ALUMINIO 1100

SOLIDIFICACION DE METALES

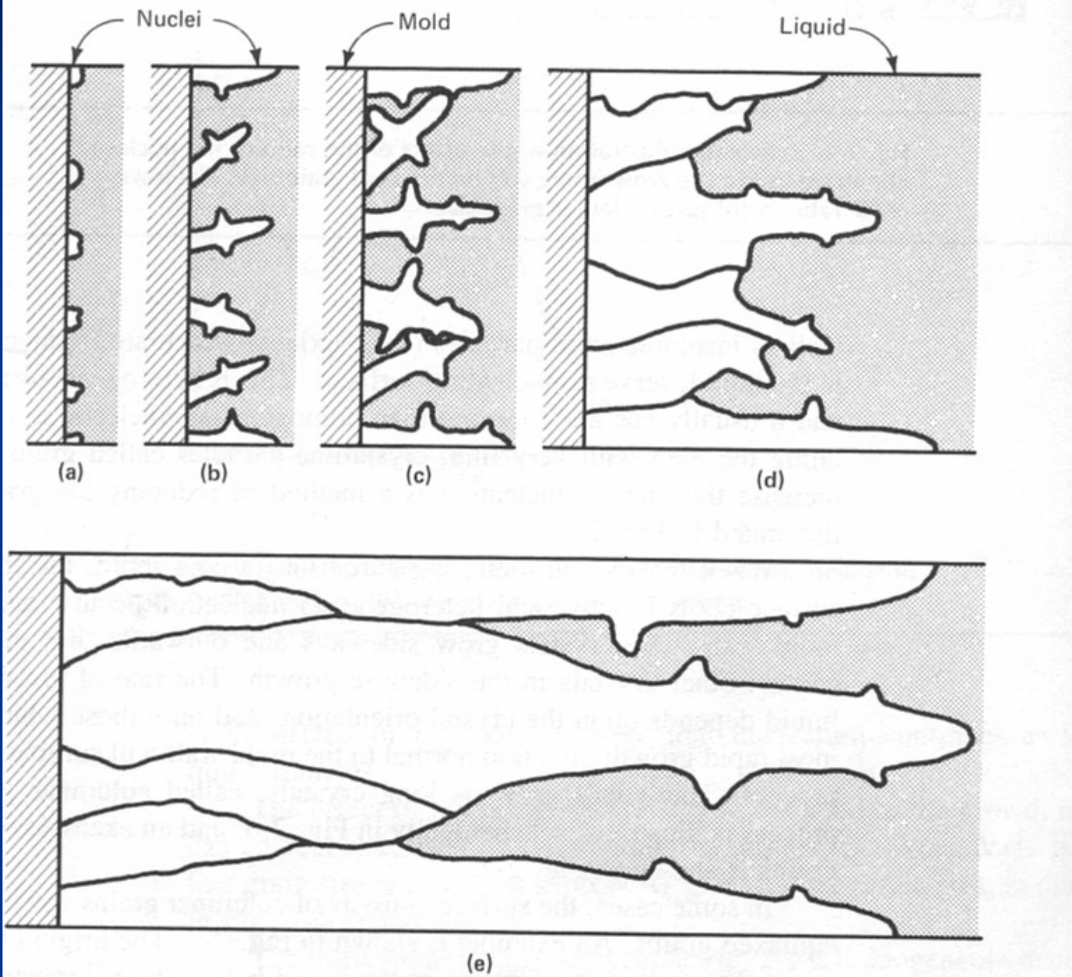

Fig. 2-6. Schematic illustration of the formation of columnar grains.

CRECIMIENTO DE GRANOS COLUMNARES

SOLIDIFICACION DE METALES

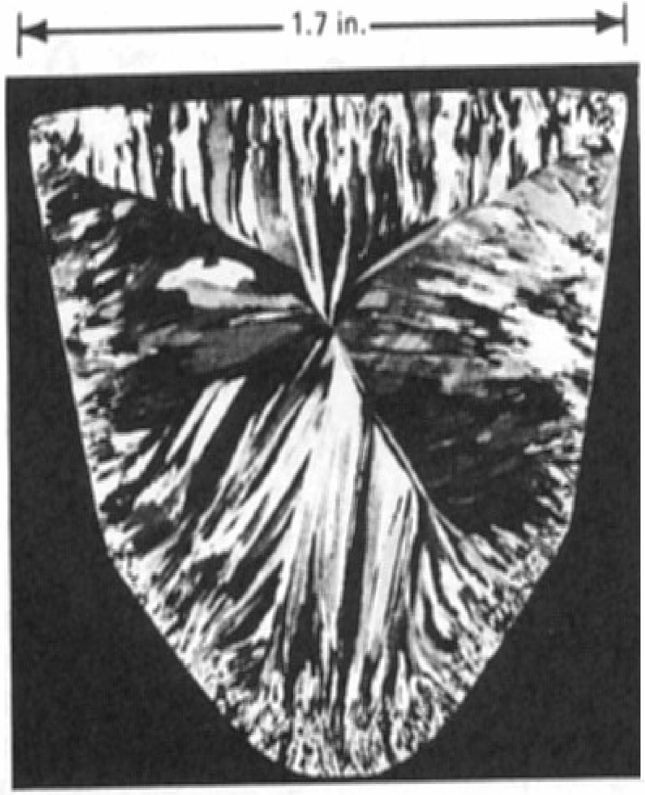

Fig. 2-7. Macrostructure of a transverse section through an ingot of commercially pure aluminum (1100 aluminum) cast by the wheel-and-belt method. Note that columnar grains have formed perpendicular to the mold wall, and also note the small grains at the surface which were outgrown by the other grains. (Adapted from same source as Fig. 2-5)

ESTRUCTURA COLUMNAR EN ALUMINIO 1100

SOLIDIFICACION DE METALES

MACROESTRUCTURA DE SOLIDIFICACION DE UN LINGOTE DE LATÓN DE CORTE LIBRE (360) MOSTRANDO GRANOS COLUMNARES CRECIENDO DESDE LA SUPERFICIE Y GRANOS EQUIAXIALES EN EL CENTRO. LA FOTO SUPERIOR ES UNA SECCION TRANSVERSAL Y LA INFERIOR CORRESPONDE AL FONDO

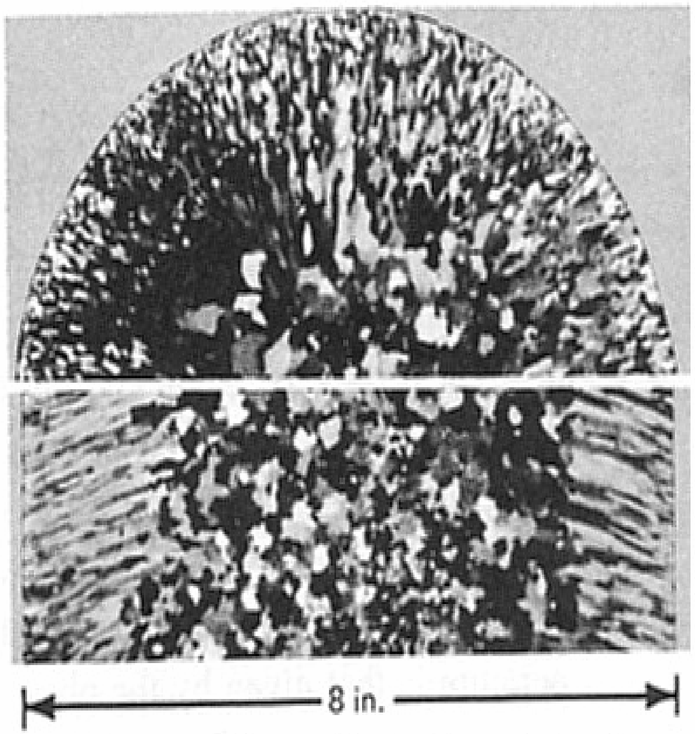

Fig. 2-8. Macrostructure of a static cast ingot of a free-cutting brass (alloy 360), showing columnar grains growing in from the surface and equiaxed grains in the center. The top picture is a transverse section, the bottom longitudinal. (Adapted from same source as Fig. 2-5)

SOLIDIFICACION DE METALES

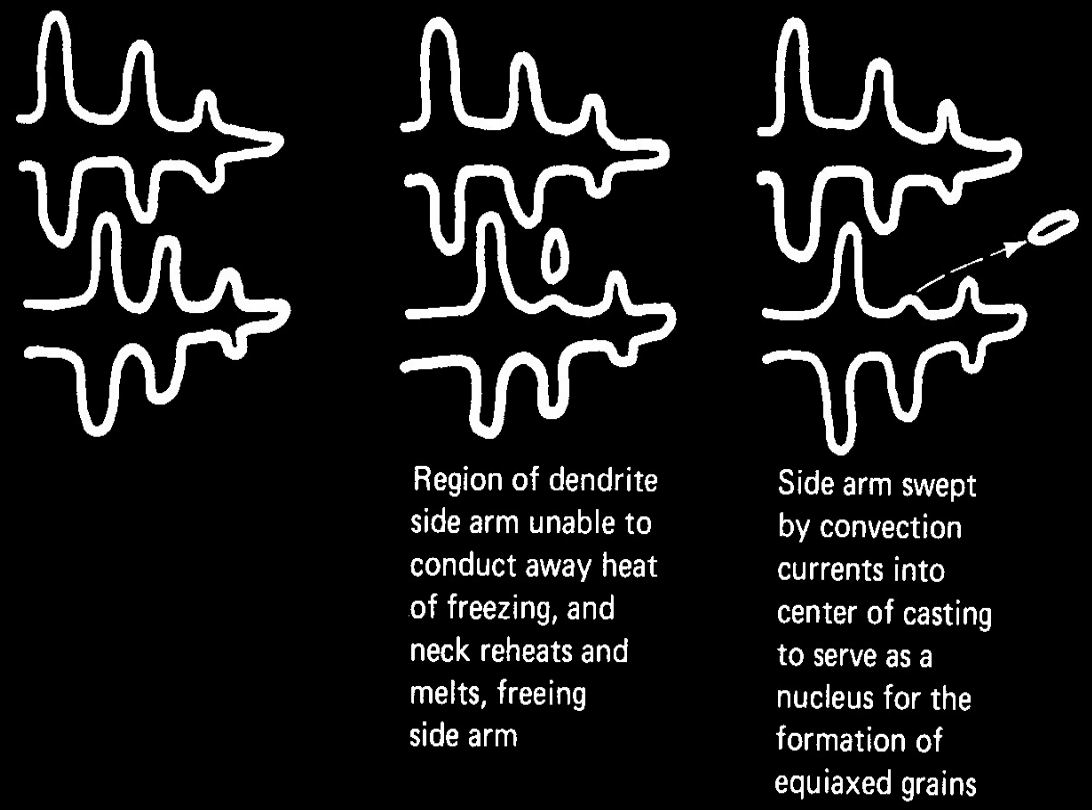

Fig. 2-9. Schematic illustration of the remelting of a side arm of a dendrite and movement of the side arm into the center of the casting to serve as the nucleus of an equiaxed grain.

REFUSION DE UN BRAZO DENDRITICO Y MOVIMIENTO HACIA EL CENTRO PARA LA CREACION DE UN NUCLEO EQUIAXIAL

SOLIDIFICACION DE METALES

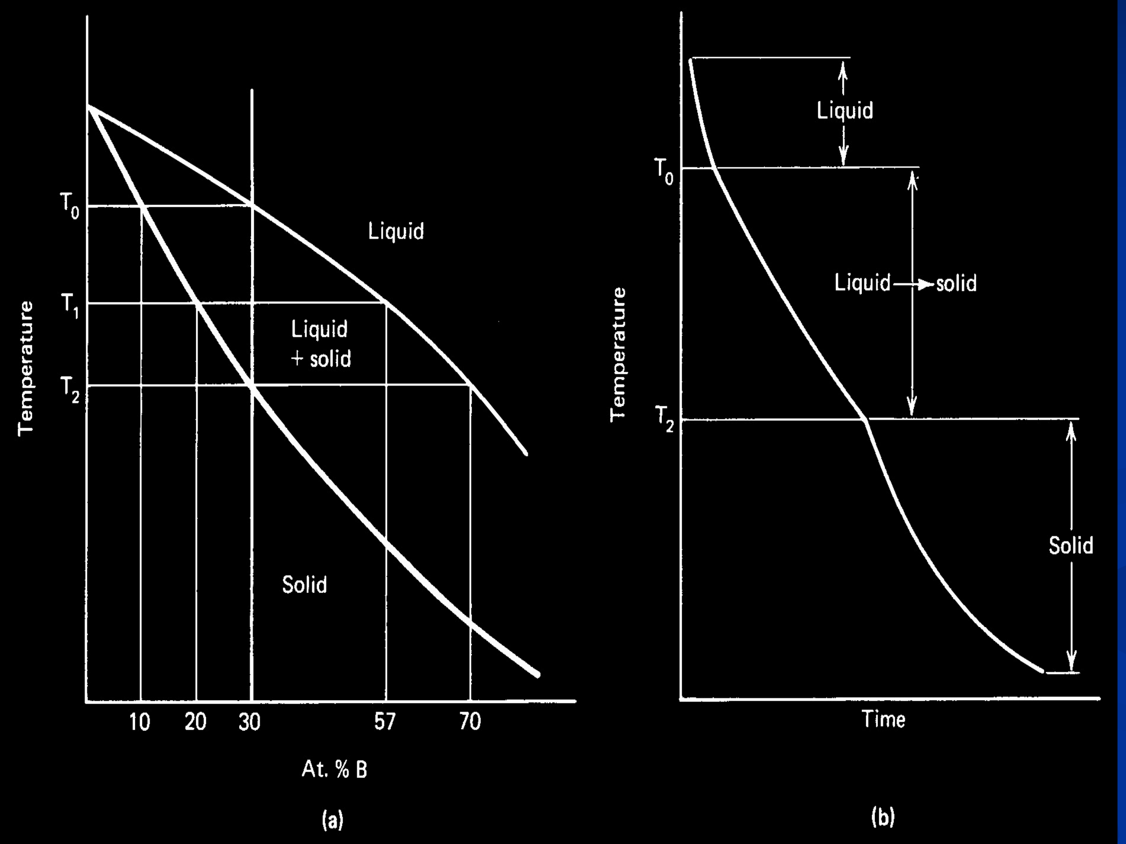

Fig. 2-10. (a) Phase diagram for system A-B in which the liquid freezes to give a single solid phase by passing through a liquid-solid region. (b) Cooling curve for a 30% B alloy.

DIAGRAMA DE FASES Y CURVA DE ENFIAMIENTO PARA UNA ALEACION BINARIA DE A-B

SOLIDIFICACION DE METALES

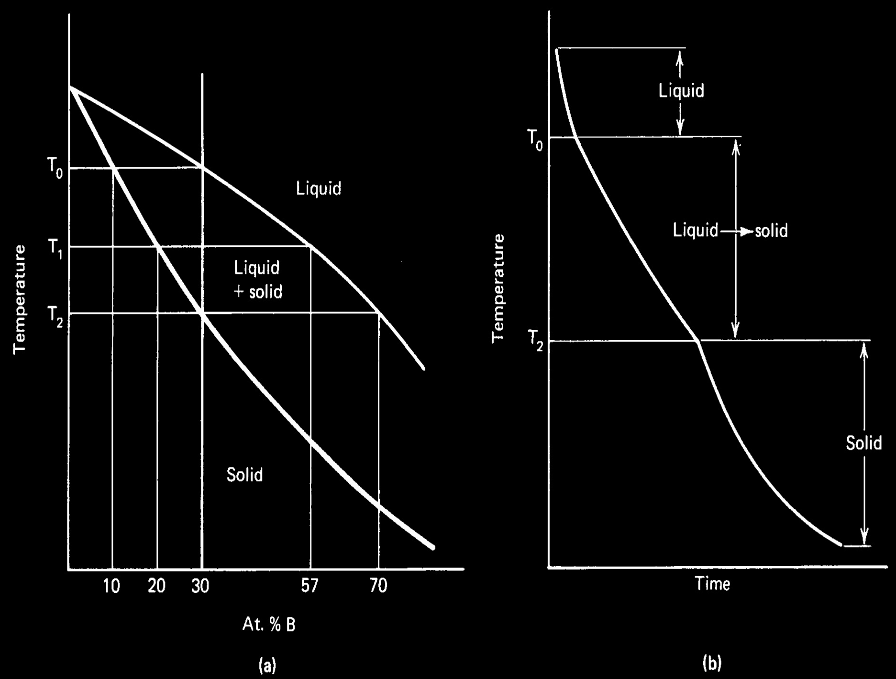

Fig. 2-10. (a) Phase diagram for system A-B in which the liquid freezes to give a single solid phase by passing through a liquid-solid region. (b) Cooling curve for a 30% B alloy.

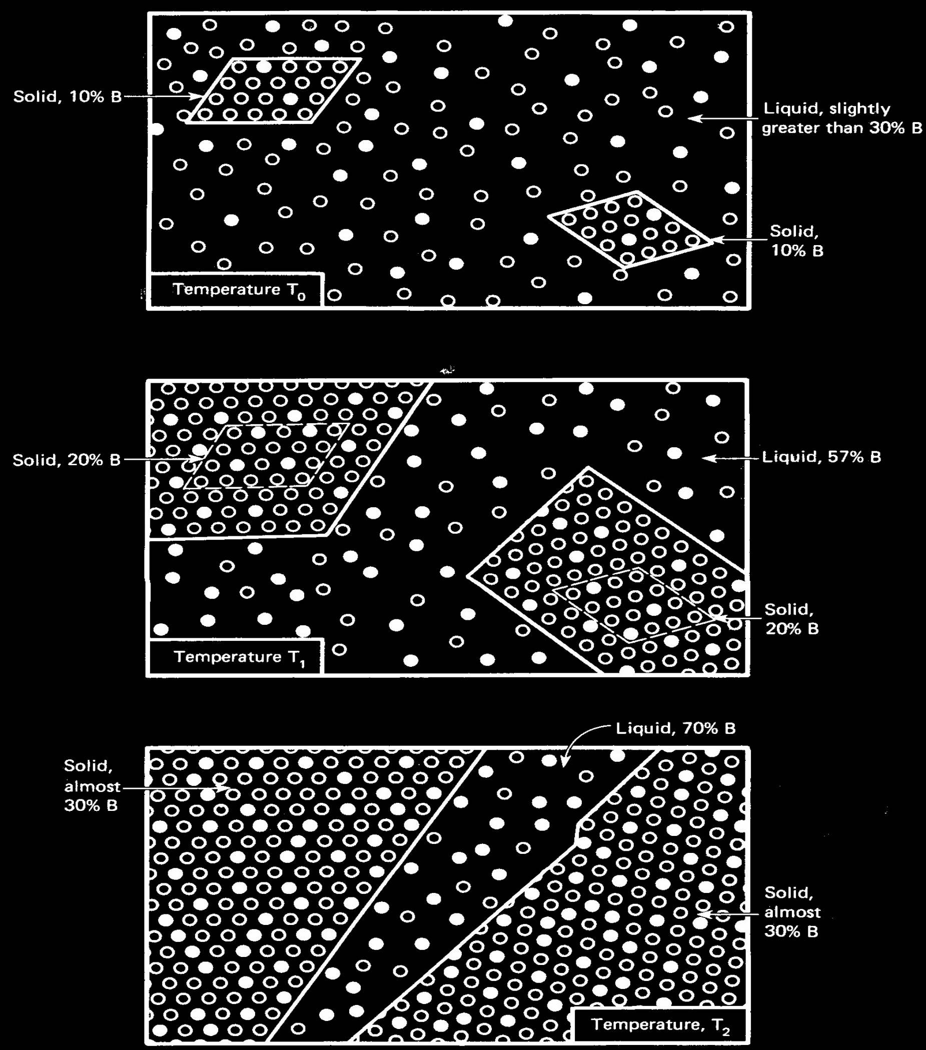

Fig. 2-11. Schematic illustration of the growth of two crystals in a 30% B alloy during equilibrium cooling. The chemical compositions of the solid and liquid are obtained from the phase diagram in Fig. 2-10(a). For simplicity, the crystals are not shown as dendrites.

ESQUEMA DE LAS ETAPAS DE SOLIDIFICACION DE UNA ALEACION BINARIA

SOLIDIFICACION DE METALES

ILUSTRACION ESQUEMATICA DEL DESARROLLO DE SEGREGACION INTERDENDRITICA

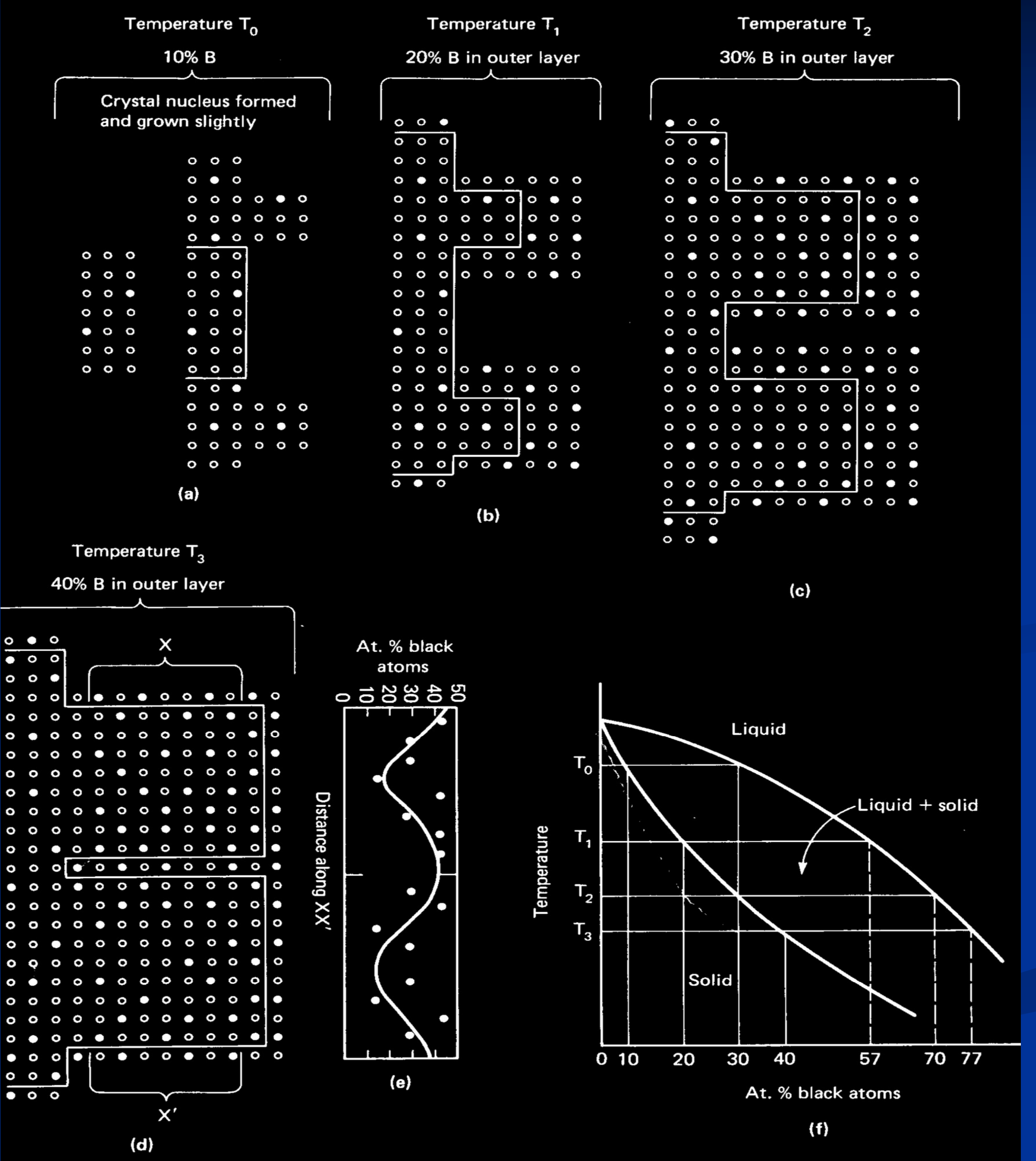

Fig. 2-12. Schematic illustration of the development of coring in a growing dendrite. See text for discussion.

SOLIDIFICACION DE METALES

FORMACION DE DENDRITAS QUE PRESENTAN SEGREGACION QUIMICA

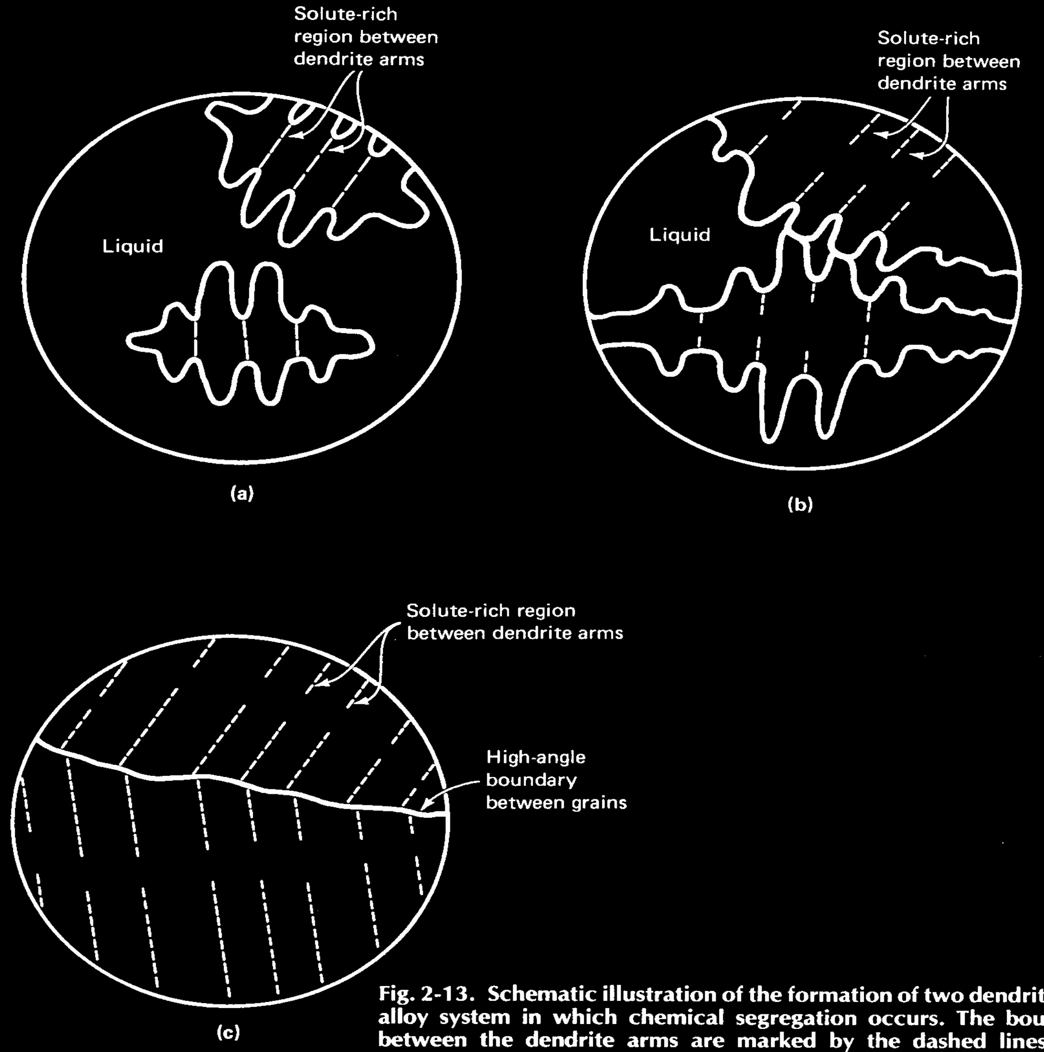

Fig. 2-13. Schematic illustration of the formation of two dendrites in an alloy system in which chemical segregation occurs. The boundaries between the dendrite arms are marked by the dashed lines; these regions are solute-rich if the alloy is 30% B (Fig. 2-12). The effect of etching a polished surface having the segregation shown in (c) is illustrated in Fig. 2-14.

SOLIDIFICACION DE METALES

REPRESENTACION ESQUEMATICA DE LA TOPOLOGIA SUPERFICIAL PRODUCTO DE SEGREGACION QUIMICA DURANTE EL CRECIMIENTO DENDRITICO

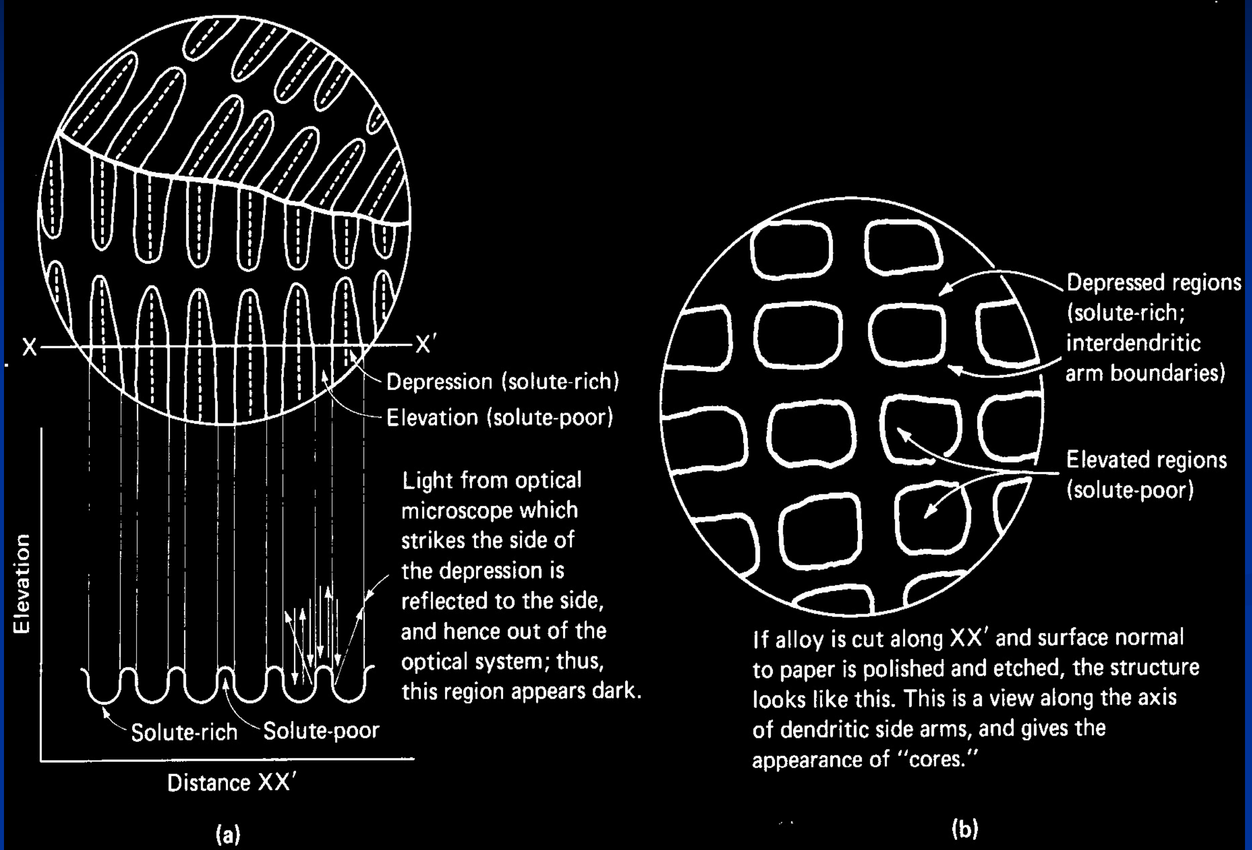

Fig. 2-14. Schematic illustration of the surface topology developed upon etching an alloy in which chemical segregation exists. If the plane of view in Fig. 2-13(c) is polished and etched, the solute-rich and solute-poor regions will be dissolved at different rates, leading to depressions (shown here along the solute-rich regions) and elevations. Upon viewing this surface with the optical microscope, the light striking the side of these regions will be reflected out of the optical system, and hence these regions appear dark. (b) Shows the appearance if the plane of cut is such that the ends of the dendrite arms are viewed.

SOLIDIFICACION DE METALES

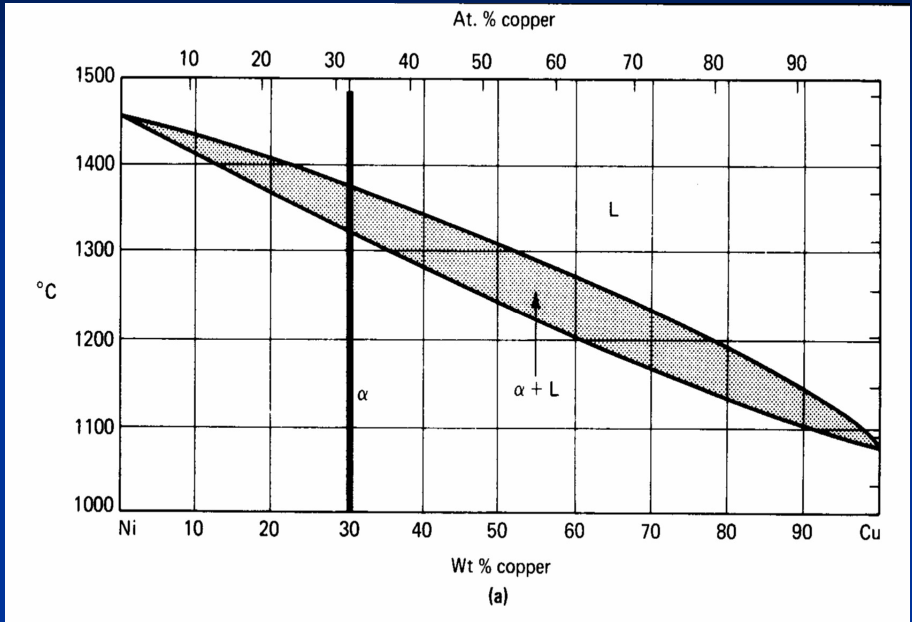

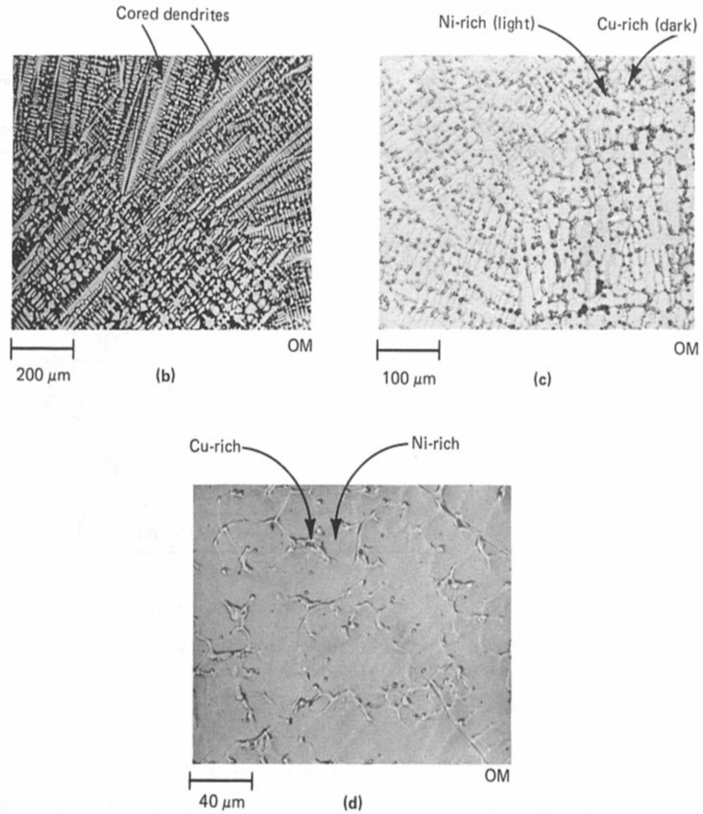

Fig. 2-15. Microstructure of a Ni-30Cu alloy which has been nonequilibrium cooled from the liquid to 20 °C. Coring is evident; this appearance originates by the mechanism described in Fig. 2-14 (especially compar with Fig. 2-14b). (Phase diagram adapted from Metals Handbook, 1948 Edition, American Society for Metals Metals Park, Ohio)

ALEACION Ni – 30 Cu MOSTRANDO SEGREGACION DENDRITICA

SOLIDIFICACION DE METALES

ALEACION Ni – Cu 30 HOMOGENIZADA A 1000 °C POR 5 h Y LUEGO ENFRIADA A 20 °C.

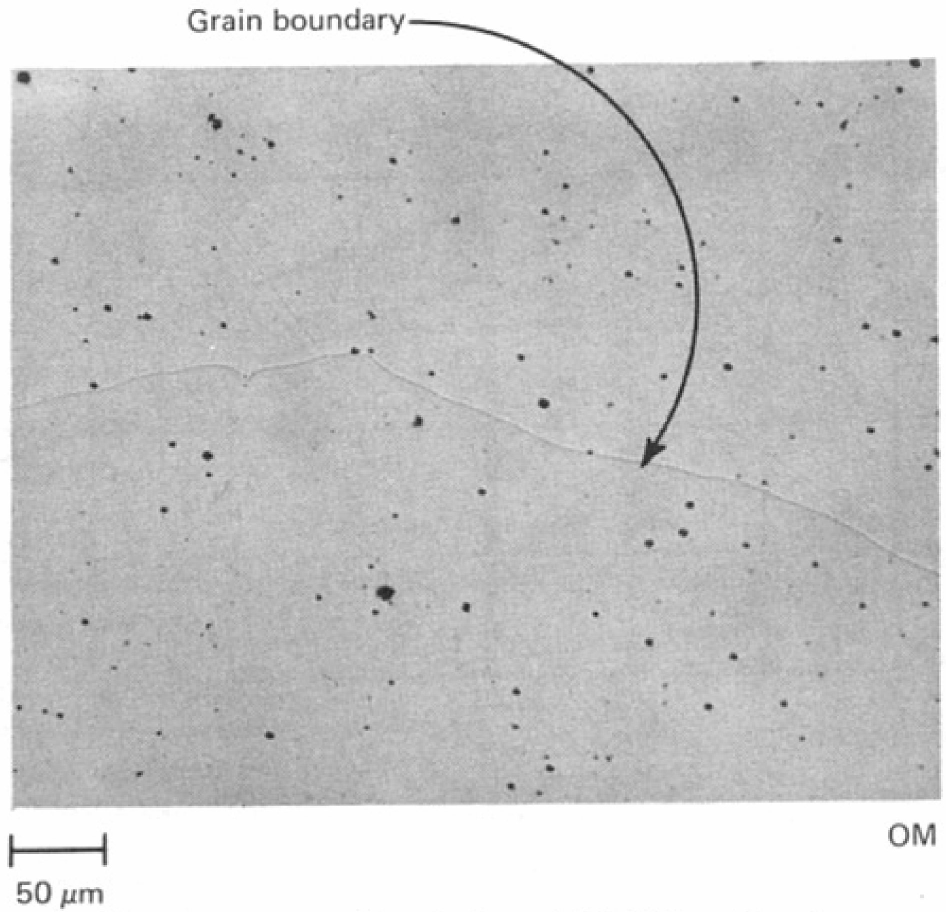

Fig. 2-16. Microstructure of a chill-cast Ni-30Cu alloy homogenized at 1000 °C for 5 h, then cooled to 20 °C. The microstructure before this heat treatment is shown in Fig. 2-15(b). The black dots are oxide inclusions and shrinkage cavities. Note the relative absence of coring.